Steel and Composite Structures, *Vol. 33, No. 5* (*2019*) *681-697*
DOI: https://doi.org/10.12989/scs.2019.33.5.681

Initial stiffness and moment capacity assessment of stainless steel composite bolted joints with concrete-filled circular tubular columns

Jia Wang*, Brian Uy [a] and Dongxu Li [b]

School of Civil Engineering, *The University of Sydney*, *Sydney*, *NSW*, *2006*, *Australia*

(*Received June 25, 2019, Revised October 25, 2019, Accepted November 18, 2019*)

Abstract. This paper numerically assesses the initial stiffness and moment capacity of stainless steel composite bolted joints with concrete-filled circular tubular (CFCT) columns. By comparing with existing design codes including EN 1993-1-8 and AS/NZS 2327, a modified component method was proposed to better predict the flexural performance of joints involving circular columns and curved endplates. The modification was verified with independent experimental results. A wide range of finite element models were then developed to investigate the elastic deformations of column face in bending which contribute to the corresponding stiffness coefficient. A new design formula defining the stiffness coefficient of circular column face in bending was proposed through regression analysis. Results suggest that a factor for the stiffness coefficient of endplate in bending should be reduced to 0.68, and more contribution of prying forces needs to be considered. The modified component method and proposed formula are able to estimate the structural behaviour with reasonable accuracy. They are expected to be incorporated into the current design provisions as supplementary for beam-to-CFCT column joints.

Keywords: stainless steel; circular column; beam-to-column joint; component method; initial stiffness; moment capacity

1. Introduction

Various advantages in stainless steel have made it develop into a structural material in building construction that possesses higher ductility, superior corrosion and fire resistance, and reduced costs in maintenance within a whole life cycle (Dai and Lam 2010, Theofanous and Gardner 2012, Averseng *et al*. 2017, Lan *et al*. 2018, Ding *et al*. 2019, Cai and Young 2019). An evident difference between stainless steel and carbon steel is the significant strain-hardening effects in stainless steel. This phenomenon contributes to a significant elongation before fracture of the material, and thus improves structural performance and avoids premature or brittle damages. Bolted steel beam-to-column joints have been classified as semi-rigid joints with sufficient ductility, and the replacement of conventional carbon steel with stainless steel can further improve their mechanical behaviour to resist extreme loading conditions, such as impact loading and seismic actions.

Regarding composite bolted joints, a wide range of literature has been found with a focus on the flexural performance of connections subjected to monotonic and cyclic loading (Lai *et al*. 2019, Costa *et al*. 2019, Li *et al*. 2019, Francavilla *et al*. 2018, Song *et al*. 2017, Amadio *et al*. 2017, Yang *et al*. 2015, Yang and Tan 2013, Qiang *et al*. 2014, Gil *et al*. 2013, Tizani *et al*. 2013, Jeyarajan and Liew 2016). Specifically, Hoang *et al*. (2014) and Zeng *et al*. (2018) investigated the moment-rotation relationships of composite joints with circular hollow columns numerically and experimentally. Structural characteristics in terms of initial stiffness and moment resistance were compared with design codes, and the corresponding design criteria were proposed to accurately predict the performance. Moreover, a series of experimental programmes, aiming to evaluate the static behaviour of bolted joints with concrete-filled circular tubular (CFCT) columns and endplates, have been conducted by Thai *et al*. (2017), Tao *et al*. (2017), Wang and Zhang (2017). The obtained test results were analysed and compared with specimens related to concrete-filled square tubular (CFST) columns. Conclusions were drawn that the flexural stiffness of joints with CFCT columns was larger than those with CFST columns.

Note that all the research mentioned above focused on the conventional carbon steel structures except the one reported by Tao *et al*. (2017), where stainless steel was only applied to columns. A full range of research needs to be implemented so as to promote a wider application of stainless steel. Accordingly, Elflah *et al*. (2019a, b) designed stainless steel beam-to-column joints with bolted endplates, where open-section columns and rectangular hollow columns were considered. The high ductility of stainless steel structures was particularly highlighted in the tests. Apart from these, limited research was found concerning the stainless steel composite joints with CFCT columns. Given the ease and economic costs of numerical methods, it is desired to develop finite element modelling to provide valuable insight into the structural forms. Meanwhile, the component method specified in EN 1993-1-8 (2005) is not able to properly predict the initial stiffness

*Corresponding author, Resaerch Associate,
E-mail: jia.wang@sydney.edu.au
[a] Professor, E-mail: brian.uy@sydney.edu.au
[b] Research Associate, E-mail: dongxu.li@sydney.edu.au

ISSN: 1229-9367 (Print), 1598-6233 (Online)

of joints with rectangular columns (Wang *et al*. 2018a, b). Thai and Uy (2016) hence proposed modified component methods by introducing deformations of column side walls in tension and compression plus column face in bending. Moreover, AS/NZS 2327 (2017) adopted the refined component methods, which were capable of predicting the initial stiffness and moment capacity of joints with hollow or CFST columns (Wang *et al*. 2019). Nonetheless, the feasibility of modified methods for estimating the performance of composite joints with CFCT columns remains pending and needs to be discussed herein.

To fill the research gap, the performance of stainless steel composite bolted joints with CFCT columns was investigated. Finite element (FE) models were developed with geometric and material nonlinearity considered. The numerical outcomes were afterwards validated by independent test results. Comparisons of initial stiffness between numerical simulations and design codes were conducted to determine if the design codes were able to provide sufficient predictions. After that, the deformations of CFCT column walls were evaluated by a large number of FE models with varied parameters such as the diameter and thickness of columns as well as the positions of bolt holes. Regression analysis was then implemented to derive new expressions for the stiffness coefficient of column walls in bending. The study was finally extended to stainless steel composite joints for broader applications.

2. Numerical modelling of beam-to-column joints

Three-dimensional finite element models of composite beam-to-column joints were developed using the general-purpose finite element package ABAQUS (2016). Those models were designed based on independent experimental specimens from Wang *et al*. (2009), Wang and Chen (2012), Thai *et al*. (2017) and Tao *et al*. (2017). The specific structural configurations are collected in Table 1. It should be noted that all specimens were made of carbon steel except CB2-1 where stainless steel was only applied to columns.

2.1 Setup of FE models

Major structural components were assigned with eight node reduced-integration solid elements (C3D8R) which are sufficient for subassembly models given that more than three layers of mesh size are guaranteed in the thickness direction. In addition, shell elements (S4R) were deployed to profiled steel sheeting, while truss elements (T3D2) were adopted for reinforcing bars. Tie restraints were utilised to simulate the boundary condition between welding seams and structural steel. The FE models were computed by an explicit solver algorithm to overcome convergence issues. Appropriate step time was determined so that it did not increase computation time or incur impacting effects due to a high speed. The impacting effect can be minimised by keeping the kinetic energy less than 5% of internal energy in total. General contact algorithm with the friction coefficient of 0.2 and hard contact strategy was selected to simulate the contact conditions. Besides, specific loading and boundary conditions were applied according to each tested specimen.

As for material properties, the stress-strain curves were extracted from each test results outlined in Table 2. The missing properties in shear connectors and profiled sheeting by Thai *et al*. (2017) can be referred to those by Tao *et al*. (2017) due to the similar configurations. Ductile damage models were ignored since this study only focused on the initial stiffness and moment capacity of the joints. As a result, elastic-plastic material characteristics without fracture were adopted for all structural steel. Additionally, plain concrete and confined concrete properties were considered for concrete slabs and concrete filled in columns respectively, and the corresponding stress-strain relationships were derived by Shams and Saadeghvaziri (1999) and Mursi and Uy (2003).

2.2 Validation of FE models and discussion

The simulation results were compared with the corresponding test outcomes in terms of moment-rotation relationships shown in Figs. 1-4. It can be seen that the finite element method was able to evaluate the flexural behaviour of bolted joints with circular columns. In particular, the ratios of numerical values to test results

Table 1 Structural configurations of specimens (Unit: mm)

Reference	Specimen	Column section $D_c \times t_c \times H$	Beam section $h_b \times b_{fb} \times t_{fb} \times t_{wb} \times L$	Endplate $D_p \times t_p$	Bolts	Shear connectors	Longitudinal reinforcing bars	Concrete slab D_{cs}
Wang *et al*. (2009)	CJM3	219×8×1400	300×150×9×6.5×1200	340×18	M16			
	CJM4	219×8×1400	300×150×9×6.5×1200	340×12	M16			
Wang and Chen (2012)	MEC1	200×10×1625	300×150×10×6×1580	540×12	M20			
	MEC2	200×10×1625	300×150×10×6×1580	540×18	M20			
Thai *et al*. (2017)	CE	273.1×9.3×1024	454×190×12.7×8.5×1388.5	544×12	M20	M19	N16	120
	CF	273.1×9.3×1024	454×190×12.7×8.5×1388.5	474×12	M20	M19	N16	120
Tao *et al*. (2017)	CB2-1	360×6×2200	304×165×10.2×6.1×1320	304×10	M20	M19	N12	120
	CB2-3	360×6×2200	304×165×10.2×6.1×1320	304×10	M20	M19	N12	120

Table 2 Material property of components

Reference	Component	Young's modulus E_0 (MPa)	Yield strength σ_{ys} / $\sigma_{0.2}$ (MPa)	Ultimate strength σ_{us}	Elongation ε_f (%)	n	m	Compressive strength σ_{uc} (MPa)
Wang *et al*. (2009)	Beam flange	196,000	262.3	377.6	17			
	Beam web	190,000	272.8	380.7	19			
	Steel tube	198,000	279.8	369.2	21			
	Endplate (12 mm)	202,000	313.0	448.4	17			
	Endplate (18 mm)	186,000	268.5	399.2	16			
	Bolt		752	946				
	Concrete	34,258						64 (Cube)
Wang and Chen (2012)	Beam flange	187,000	349.3	492	16.5			
	Beam web	216,000	312.5	508.3	17.4			
	Steel tube	194,000	331.8	484.5	18.2			
	Endplate (12 mm)	198,000	323.3	436.7	31.0			
	Endplate (18 mm)	193,000	274.4	414.4	24.8			
	Bolt		900	1000				
	Concrete	31,8778						44.3 (Cube)
Thai *et al*. (2017)	Beam flange	200,000	328	475	30			
	Beam web	200,000	387	498	27			
	Endplate	200,000	358	494	28			
	Steel tube	200,000	460	526	23			
	Reinforcement	200,000	565	660	15			
	Bolt	200,000	820	966	30			
	Shear connector*	203,941	375	517	24.4			
	Profiled sheeting*	198,494	352	535	4.5			
	Concrete							47.1 (Cylinder)
Tao *et al*. (2017)	Beam flange	198,494	352	535	25.2			
	Beam web	203,765	370	534	24.5			
	Carbon steel tube	206,338	379	473	25.8			
	Stainless steel tube	200,663	367	732	49.3			
	Endplate	206,298	388	506	30.4			
	Profiled sheeting	198,494	352	535	4.5			
	Bolt	218,871	890	953	15.3			
	Reinforcement	200,371	538	653	9.0			
	Shear connector	203,941	375	517	24.4			
	Concrete							43.8 (Cylinder)
Elflah *et al*. (2019a, 2019b)	Beam flange	196,500	248	630	66	5.2	2.37	
	Beam web	205,700	263	651	65	6.7	2.41	
	Steel tube	200,020	507	730	51	8.4	3.43	
	Endplate	195,000	276	636	51	11.05	2.51	
	Bolt	191,500	617	805	12	17.24	3.68	
Gardner *et al*. (2016)	Reinforcement	202,600	480	764	38.6			

Note: The material properties in shear connector and profiled sheeting marked with "" in Thai *et al*. (2017) can be referred to those in Tao *et al*. (2017)

regarding the initial stiffness and moment capacity, which are two critical parameters for beam-to-column joints, remained between 0.92-1.18 and 0.99-1.12. At the end of some curves, discrepancies happened between FEM and test results. These discrepancies could be ignored since the numerical method did not consider damages of models and more attention was focused on the initial stiffness and moment capacity in this study. Overall, the finite element

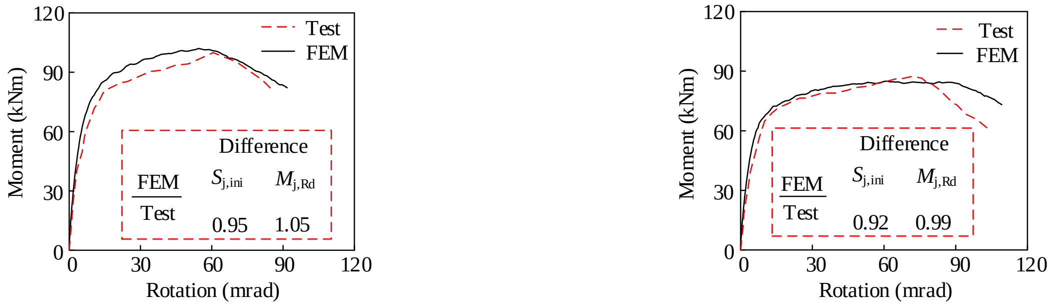

(a) CJM3 (b) CJM4

Fig. 1 Comparisons between FEM and test results by Wang *et al*. (2009)

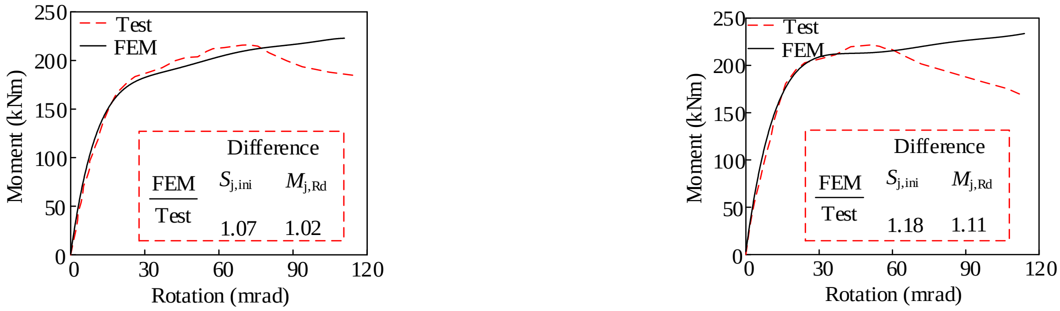

(a) MEC1 (b) MEC2

Fig. 2 Comparisons between FEM and test results by Wang and Chen (2012)

(a) CE (b) CF

Fig. 3 Comparisons between FEM and test results by Thai *et al*. (2017)

Table 3 Rotational stiffness of joints

Specimen	Carbon steel		Stainless steel	
	$\frac{S_{j,2/3}}{S_{j,ini}}$	$\frac{S_{j,1/2}}{S_{j,ini}}$	$\frac{S_{j,2/3}}{S_{j,ini}}$	$\frac{S_{j,1/2}}{S_{j,ini}}$
CJM3	0.84	0.87	0.84	0.86
CJM4	0.80	0.86	0.79	0.85
MEC1	0.80	0.88	0.74	0.93
MEC2	0.83	0.91	0.76	0.87
CE	0.83	0.86	0.79	0.85
CF	0.81	0.90	0.76	0.90
CB2-1	0.84	0.90	0.64	0.88
CB2-3	0.84	0.90	0.64	0.88

method is reliable to estimate the structural performance of beam-to-column joints with concrete-filled circular columns. Therefore, further simulation can proceed to investigate the behaviour of beam-to-circular column joints made of stainless steel.

Eight specimens remained the same configuration, while all carbon steel was replaced by stainless steel. Material properties of stainless steel were mainly collected from independent test results by Elflah *et al*. (2019a, b). The stress-strain relationship of stainless steel reinforcing bar was obtained from research by Gardner *et al*. (2016). The complete stress-strain curves can be achieved by formulae (Ramberg and Osgood 1943, Mirambell and Real 2000) as follows

$$\varepsilon_{nom} = \frac{\sigma_{nom}}{E_0} + 0.002\left(\frac{\sigma_{nom}}{\sigma_{0.2}}\right)^n, \quad \sigma_{nom} < \sigma_{0.2} \tag{1}$$

$$\varepsilon_{nom} = \frac{(\sigma_{nom} - \sigma_{0.2})}{E_{0.2}} + \left(\varepsilon_u - \varepsilon_{0.2} - \frac{\sigma_u - \sigma_{0.2}}{E_{0.2}}\right) \times \left(\frac{\sigma - \sigma_{0.2}}{\sigma_u - \sigma_{0.2}}\right)^m + \varepsilon_{0.2}, \quad \sigma_{nom} > \sigma_{0.2} \tag{2}$$

$$n = ln\left(20 - \frac{\sigma_{0.2}}{\sigma_{0.1}}\right) \tag{3}$$

$$E_{0.2} = \frac{E_0}{1 + \frac{0.002n}{E_0/\sigma_{0.2}}} \tag{4}$$

where n and m are exponential parameters and can be determined from test results.

All numerical results including moment capacity and initial stiffness were collected in Tables 5 and 6. Meanwhile, two typical moment-rotation relationships of steel joints and composite joints were illustrated in Fig. 5. It is found that the moment capacity ($M_{\mathrm{j,Rd}}$) of stainless steel joints was normally lower than that of carbon steel due to the lower value of yield strength in stainless steel, and the percentage difference could reach 28%. Note that ultimate moment resistance of stainless steel joints could be higher than that of carbon steel joints if the ultimate strength of stainless steel was larger. On the other hand, the initial stiffness between both steels were similar owing to a similar value of Young's modulus, and the percentage difference remain with 10%.

Fig. 5 and Table 3 describes a comparison of rotational stiffness which is the gradient of secant line between the origin and different points. It can be seen that the ratio of rotational stiffness at two thirds of moment capacity to initial stiffness remained more than 0.8 for carbon steel but fluctuated from 0.64 to 0.84 for stainless steel. It is well understood that the determination of initial stiffness based

(a) CB2-1 (b) CB2-3

Fig. 4 Comparisons between FEM and test results by Tao *et al.* (2017)

Table 4 Stiffness coefficient of basic components

	EN 1993-1-8 & EN 1994-1-1	AS/NZS 2327
Column web panel in shear	∞	∞
Column web in compression	∞	∞
Column web in tension	$k_3 = 0.7b_{eff,t,wc}t_{wc}/d_c$	∞
Column flange in bending	$k_4 = 0.9l_{eff}{t_{fc}}^3/m^3$	$k_4 = k\dfrac{16{t_c}^3}{L^2}\dfrac{\alpha + (1-\beta)\tan\theta}{(1-\beta)^3 + 10.4(1.5-1.63\beta)/\mu^2}$
Endplate in bending	$k_5 = 0.9l_{eff}{t_p}^3/m^3$	$k_5 = 0.9l_{eff}{t_p}^3/m^3$
Bolts in tension	$k_{10} = 1.6A_s/L_b$	$k_{10} = 1.6A_s/L_b$
Reinforcing bars in tension	$k_{s,r} = A_{s,r}/(3.6h)$ (Single-sided) or $k_{s,r} = A_{s,r}/(0.5h)$ (Double-sided)	$k_{s,r} = A_{s,r}/(3.6h)$ (Single-sided) or $k_{s,r} = A_{s,r}/(0.5h)$ (Double-sided)

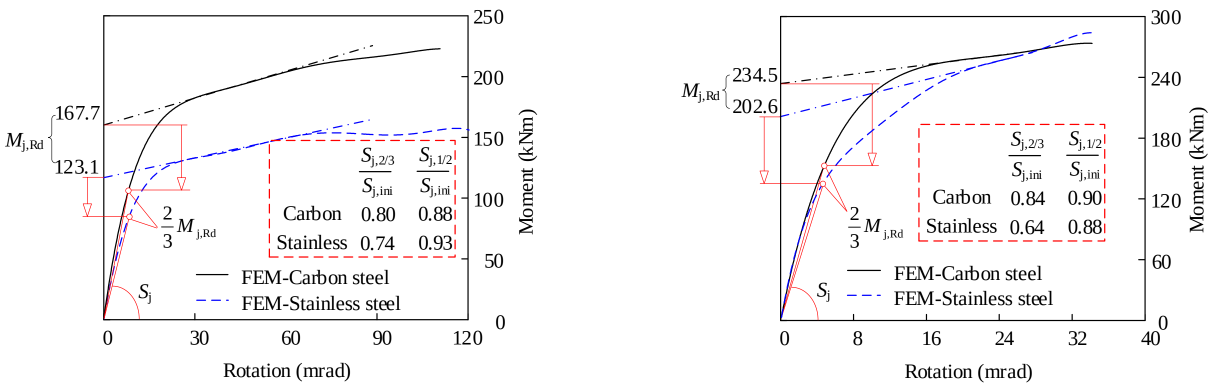

(a) MEC1 (b) CB2-1

Fig. 5 Moment-rotation relationships of joints with carbon steel and stainless steel

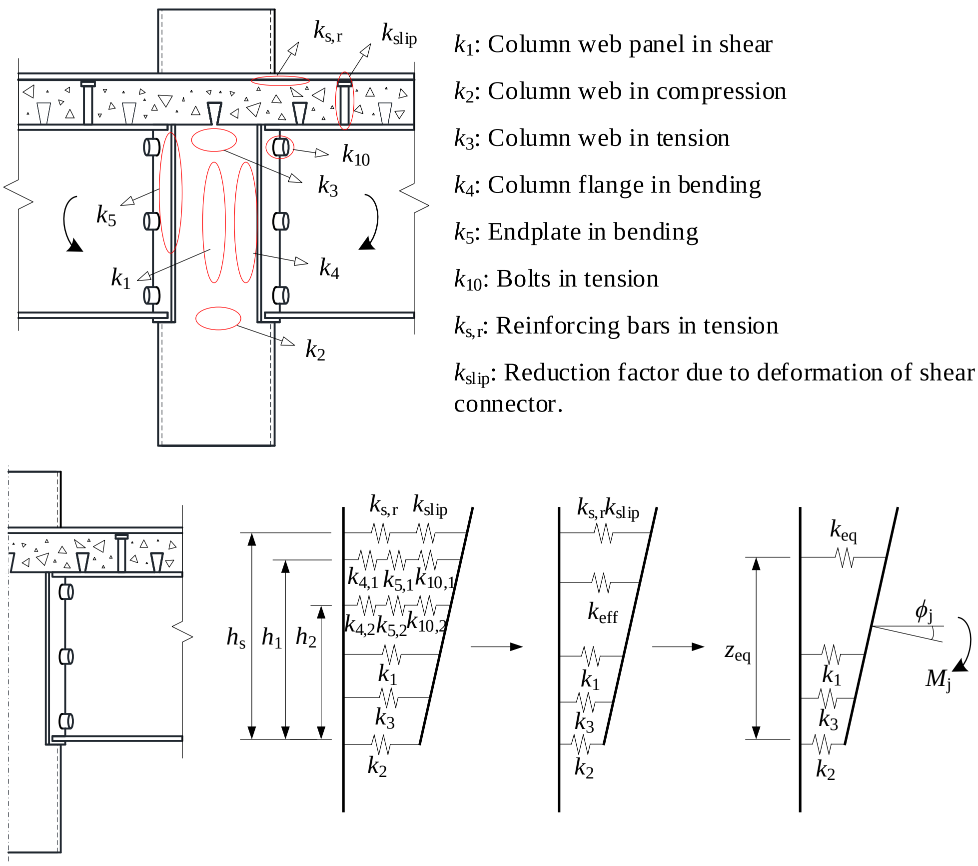

Fig. 6 Component method

on numerical results is normally dominated by the elastic response of joints. The evident fluctuation for stainless steel suggested that the elastic moment range was less than two thirds of moment capacity. If comparing the secant stiffness at a half of moment capacity and initial stiffness, the ratio improved significantly ranging from 0.85 to 0.93 for stainless steel. As a result, the elastic moment of stainless steel joints should be within a half of moment capacity, and the initial stiffness needs to be acquired within this range. Song *et al*. (2019) clarified that the stiffness value can be defined by the moment and rotation corresponding to the crack of concrete slab whereas joints still behaved elastically. In this study, the initial stiffness was obtained by the elastic moment which was less than 10% of moment capacity to guarantee the accuracy.

3. Assessment of design provisions

The design guidance for beam-to-column bolted joints is available in EN 1993-1-8 (2005), EN 1994-1-1 (2004) and AS/NZS 2327 (2017). The preliminary principle is to divide the integral parts into individuals that are subjected to various loading conditions as indicated in Fig. 6. The mechanical response of each can be obtained by simplified formulae, and afterwards these mechanical responses are assembled in the form of stiffness coefficients or moments aiming to determine the initial stiffness and moment capacity. This is the basic procedure of component method that has been verified as a reliable and simple method to evaluate the structural performance of joints (Liew *et al*. 2004, Wang *et al*. 2010, Francavilla *et al*. 2018, Díaz *et al*. 2018).

3.1 Moment capacity ($M_{j,Rd}$)

The moment capacity can be determined by defining the weakest component that experienced yielding firstly. In this case, the design resistance of each component was initially obtained based on design codes, and the smallest value was then selected to multiply by a lever arm. According to EN 1993-1-8 (EC3), the moment capacity is straightforwardly defined to be the maximum moment in the moment-rotation curve as shown in Fig. 7. This is because an elastic-perfectly plastic behaviour of steels is assumed in the provision and the resistance of components may not increase once reaching the yield strength. However, due to the effect of strain hardening and contribution of ultimate strength, the moment-rotation curve can experience an increase to some extent before failure. Therefore, it is desired to find the moment capacity in the moment-rotation curve that could characterise the yielding behaviour of joints in a convenient and accurate manner. Through literature review, it is found that Yee and Melchers (1986) proposed a full-range moment-rotation curve as follows which is similar as the actual curve in Fig. 7.

$$M = M_{j,Rd}\left[1 - exp\left(\left(-S_{j,ini} + S_{j,pl} - C\varphi\right)\frac{\varphi}{M_{j,Rd}}\right)\right] + S_{j,pl}\varphi \quad (5)$$

Table 5 Comparison of moment capacity between FEM and design provisions (Unit: kNm)

Specimen	Carbon steel							Stainless steel						
	$M_{j,Rd}$ (FEM)	$M_{j,Rd}$ (EC3)	Weakest part	$M_{j,Rd}$ (AS2327)	Weakest part	EC3/FEM	AS2327/FEM	$M_{j,Rd}$ (FEM)	$M_{j,Rd}$ (EC3)	Weakest part	$M_{j,Rd}$ (AS2327)	Weakest part	EC3/FEM	AS2327/FEM
CJM3	77.1	31.5	A	29.2	A	0.41	0.38	76.2	35.5	A	47.1	C	0.47	0.62
CJM4	69.6	31.5	A	29.2	A	0.45	0.42	71.6	35.5	A	38.8	C	0.50	0.54
MEC1	167.7	87.8	C+A	94.9	C+A	0.52	0.57	123.1	68.3	C+C	68.3	C+C	0.55	0.55
MEC2	208.3	108.5	C+A	115.6	C+A	0.52	0.55	150.4	100.5	C+A	111.9	C+C	0.67	0.74
CE	593.5	557.0	A+A	571.9	A+A	0.94	0.96	432.7	416.9	A+A	430.7	A+A	0.96	1.00
CF	530.3	460.6	A	462.1	A	0.87	0.87	415.1	361.8	A	367.9	A	0.87	0.89
CB2-1	234.5	169.1	A	165.9	A	0.72	0.71	202.6	158.6	A	155.5	A	0.78	0.77
CB2-3	234	169.7	A	166.4	A	0.73	0.71	196.0	153.7	A	151.5	A	0.78	0.77
Mean						0.64	0.65						0.70	0.74
SD						0.18	0.19						0.17	0.15

*Note: Weakest part A for column flange in bending; B for column web in tension; C for endplate in bending; D for Beam web in tension. C+A denotes weakest part C occurs in the first bolt row and part A occurs in the second bolt row, this normally happens in joints with extended endplates

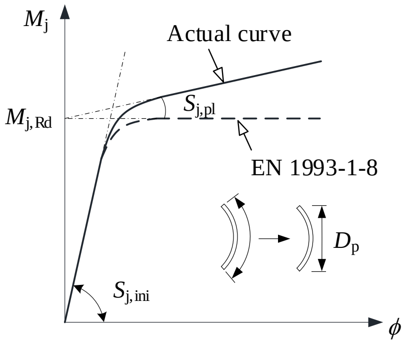

Fig. 7 Definition of moment-rotation relationship

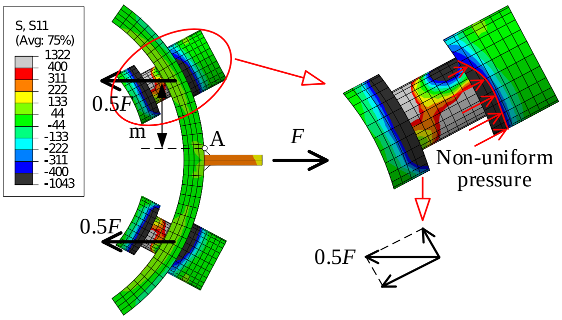

Fig. 8 Stress distributions of T-stub model

where $S_{j,pl}$ is the strain-hardening stiffness; C is the rate of decay parameter.

This analytical formula has been validated to be able to estimate the performance of beam-to-column joints reasonably well by Wang *et al*. (2018a, b). If the rotation of joints (ϕ) is large enough, Eq. (5) could be adapted as

$$M = M_{j,Rd} + S_{j,pl}\varphi \tag{6}$$

It can be seen that Eq. (6) describes a straight line in which the moment capacity can be obtained by taking ϕ as 0. As a result, the moment capacity was defined by extending the strain-hardening stiffness to y-axis as indicated in Fig. 7.

Comparing EN 1993-1-8 and AS/NZS 2327, the difference of design codes defining the moment capacity lies in the design resistance of column face in bending for CFT columns and the effective width of column web or beam web in tension. This is because EN 1993-1-8 has not involved bolted joints with tubular columns. In addition, the column flange is assumed as stiffened one to determine the effective length of CFT column flange in EN 1993-1-8. The dimensions of curved components such as the width of endplates were taken as the projected length as shown in Fig. 7.

A comparison between numerical results and design provisions was made and summarised in Table 5. It is noted that predictions by both design codes are basically similar. However, they evidently underestimate the moment capacity of joints with circular columns, especially the joints without concrete slabs. According to the weakest part predicted by design codes, it can be seen that most of the moment capacity values are attributed to yielding of column flange in bending, and the others are owing to the endplate in bending. If the column flange in bending dominates the resistance, it could underestimate the moment capacity by 59% for EN 1993-1-8 and 62% for AS/NZS 2327. Besides, the percentage difference could be 48% and 46% if the endplate in bending is the weakest part. It is well understood that the resistance of both components can be determined based on T-stub model in EN 1993-1-8. As such, the current T-stub model is not able to predict the yielding strength of circular components. One reason could be hoop stresses generated in the curved tube which result in an increase of resistance. As for endplate in bending, the capacity related to the complete yielding of T-stub flange is estimated too low. Fig. 8 denotes that more prying forces

Table 6 Comparison of initial stiffness between FEM, design provisions and modified method (Unit: kNm/rad)

Specimen	Carbon steel							Stainless steel						
	$S_{j,ini}$ (FEM)	$S_{j,ini}$ (EC3)	$S_{j,ini}$ (AS2327)	$S_{j,ini}$ (Mod.)	$\frac{EC3}{FEM}$	$\frac{AS2327}{FEM}$	$\frac{Mod.}{FEM}$	$S_{j,ini}$ (FEM)	$S_{j,ini}$ (EC3)	$S_{j,ini}$ (AS2327)	$S_{j,ini}$ (Mod.)	$\frac{EC3}{FEM}$	$\frac{AS2327}{FEM}$	$\frac{Mod.}{FEM}$
CJM3	13,084	11,233	11,345	12,028	0.86	0.87	0.92	12,645	10,952	11,061	11,727	0.87	0.87	0.93
CJM4	10,497	7,881	7,960	10906	0.75	0.76	1.04	9,901	7,684	7,761	10634	0.78	0.78	1.07
MEC1	16,579	22,998	20,830	16,515	1.39	1.26	1.00	16,771	23,603	21,378	16,949	1.41	1.27	1.01
MEC2	24,250	35,375	31,231	25,631	1.46	1.29	1.06	24,794	36,305	32,053	26,305	1.46	1.29	1.06
CE	116,827	101,558	99,990	111,149	0.87	0.86	0.95	117,844	108,292	106,621	118,753	0.92	0.90	1.01
CF	93,128	82,341	82,291	86,966	0.88	0.88	0.93	102,977	87,802	87,748	92,916	0.85	0.85	0.90
CB2-1	46,899	29,893	29,840	43,453	0.64	0.64	0.93	45,450	30,282	30,228	44,104	0.67	0.67	0.97
CB2-3	46,899	29,893	29,851	43,427	0.64	0.64	0.93	45,450	30,282	30,239	44,078	0.67	0.67	0.97
Mean					0.94	0.90	0.97					0.95	0.91	0.99
SD					0.30	0.23	0.05					0.29	0.23	0.06

occurred in the circular T-stub flange model leading to the non-uniform stress distributions and a reduced lever arm between the centre of bolt and Point A. As a result, it is desired to modify the T-stub model by amplifying the contribution of prying forces for better predictions of circular joints in the future. Meanwhile, more experimental programmes are recommended to calibrate the modification.

3.2 Initial stiffness ($S_{j,ini}$)

In accordance with design codes, seven components contribute to the initial stiffness of composite bolted joints including the column web panel in shear, column web in tension and compression, column flange in bending, endplate in bending, bolts in tension and reinforcing bars in tension. The formulae of stiffness coefficient for each component are collected in Table 4. It is clear to see that the stiffness coefficient of CFST column flange in bending is provided specially by AS/NZS 2327, while only the open-section column is covered by EN 1993-1-8. As for CFST columns, the column web panel in shear and column web in compression are regarded as rigid parts in which the stiffness coefficients are infinite. It is noted that AS/NZS 2327 also ignores the contribution of column web in tension for concrete-filled columns.

The initial stiffness of eight specimens as well as the numerical models with stainless steel mentioned in Section 2 was estimated by the design provisions. The predictions are summarised in Table 6. It is found that the initial stiffness of carbon steel structures and stainless steel structures is approximately similar. The comparison between specimens and standards suggests that EN 1993-1-8 and AS/NZS 2327 are not reliable to provide relatively accurate estimations on the initial stiffness of beam-to-CFCT column joints with carbon steel or stainless steel. The standard deviations are relatively high, which indicates a high level of discretisation of the predictions. The initial stiffness of MEC1 and MEC2 is overestimated by design codes because standards normally provide high predictions on the stiffness of column flange in bending under a large thickness and small diameter of column. This will be specified in Section 5.1. However, in most cases, design codes significantly underestimate the initial stiffness of the composite bolted joints due to various reasons. Firstly, the stiffness coefficient of circular columns differs from that of square or open-section columns and it could be underestimated. Besides, there exist variations in defining the stiffness coefficient of the curved and commonly-used endplate in bending. As mentioned in Section 3.1, significant prying forces were observed in the curved T-stub model. More rational factors should be proposed since the stiffness coefficient of endplate in bending was derived based on a standard T-stub model. Also, the deformation direction of bolts did not align with the direction of tensile force explained in Fig. 8. This contributes to diverting part of the tensile force and leads to higher stiffness of bolts in tension. Regarding composite joints with concrete slabs, profiled steel sheeting can provide additional stiffness given that sheeting ribs were placed along the direction of beam flanges.

Accordingly, it is recommended to modify the existing design provisions for a better evaluation of bolted joints with CFCT columns.

4. Modification of design provisions

4.1 Endplate in bending

Weynand *et al*. (1996) elaborated the derivation of stiffness coefficient of endplate in bending based on the T-stub model. As such, the mechanical response of curved T-stub model was created as shown in Fig. 9. The bending moment at Point B can be obtained by reactions, namely $M_B = 0.63F\cdot\text{m} - 0.13 \times (1.25 + 1)F\cdot\text{m} = 0.3375F\cdot\text{m}$. When the first plastic hinge occurred at Point B, the maximum elastic force can be expressed as

$$F_{el} = \frac{M_{el}}{0.3375m} = \frac{1}{0.3375m} \times \frac{l_{eff,ini}t^2\sigma_y}{4} = \frac{l_{eff,ini}t^2\sigma_y}{1.35m} \tag{7}$$

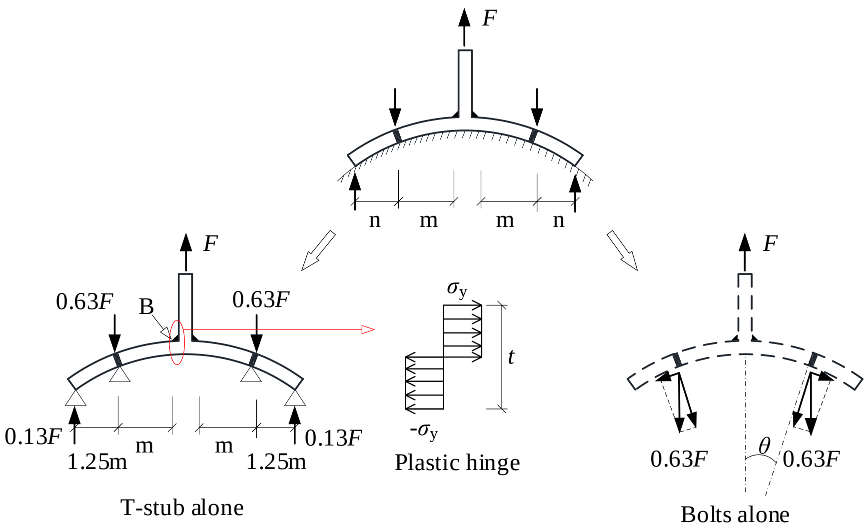

Fig. 9 T-stub model (Adapted from Weynand *et al*. 1996)

When failure developed such as yielding of flange or bolts, the failure force can be represented by

$$F_{Rd} = \frac{l_{eff} t^2 \sigma_y}{m} \tag{8}$$

In accordance with EN 1993-1-8, the ratio of maximum elastic bending moment to moment capacity ($M_{\mathrm{el}}/M_{\mathrm{Rd}}$) equals to 2/3, which can be applied to the relationship between F_{el} and F_{Rd}. However, as mentioned in Section 2.2, it is found from the moment-rotation relationships in Fig. 5 that the ratio of $M_{\mathrm{el}}/M_{\mathrm{Rd}}$ should be less than 2/3, and a value of 0.5 can conservatively reflect the fact for joints with circular columns. Therefore, the failure force F_{Rd} can be converted by Eq. (7)

$$F_{Rd} = 2F_{el} = \frac{l_{eff,ini} t^2 \sigma_y}{0.675m} \tag{9}$$

Based on Eqs. (8) and (9), the elastic effective length can be derived as

$$l_{eff,ini} = 0.675 l_{eff} \approx 0.68 l_{eff} \tag{10}$$

In this case, the stiffness coefficient of endplate in bending can be modified as

$$k_5 = \frac{0.68 l_{eff} t^3}{m^3} \tag{11}$$

It can be seen that the stiffness of curved endplates decreases compared with that of standard endplates.

4.2 Bolts in tension

Fig. 9 depicts the mechanical response of bolts in tension. It is noted that a small portion of tension was diverted in the form of frictions or bearing on bolt shank. As a result, the actual stiffness coefficient of bolts in tension is derived by

$$k_{10} = \frac{1.6 A_s}{L_b \cos\theta} \tag{12}$$

The modified stiffness coefficient suggests that the stiffness of bolts in tension increases to some extent.

4.3 Profiled sheeting in tension

As mentioned, profiled steel sheeting could contribute to the initial stiffness if the sheeting rib is placed along the direction of beam flanges. For simplicity, it is combined with reinforcement in tension, and the related stiffness coefficient can be determined based on EN 1994-1-1. It is noteworthy that the effective width of concrete slab and slips of shear connectors need to be considered for the profiled sheeting in tension.

4.4 Column face in bending

Since the stiffness coefficient of rectangular columns in AS/NZS 2327 and stiffened columns in EN 1993-1-8 cannot rationally predict the deformation of circular columns, an attempt to compute the stiffness coefficient of CFCT columns was made by finite element analysis. Eight column models were developed separately to simulate the deformations of columns in the joints mentioned above. Fig. 10(a) describes the typical geometric configurations of CFCT columns in which two bolt holes in one row were arranged. The ratio of column length to diameter was set as 4 such that the global flexural stiffness of column was strong enough in case of slenderness limit effects (Thai and Uy 2016). Meanwhile, due to the contribution of infilled concrete, the deformation of column face in bending at side A could be independently determined by the loads applied at side A as shown in Fig. 10(a), while the effect of loads at side B can be ignored. The assumption has been verified by numerical results. This study herein adopted the column with single side loaded for simplicity. A pair of loads were applied to two reference points respectively, which were bonded to bolt holes via tie constraint boundary conditions.

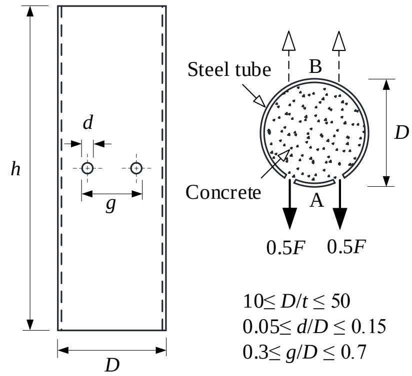

(a) Geometric configurations

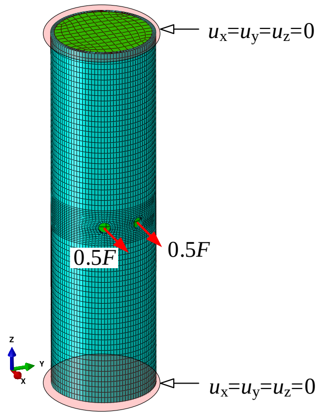

(b) Finite element model

Fig. 10 Details of CFCT column

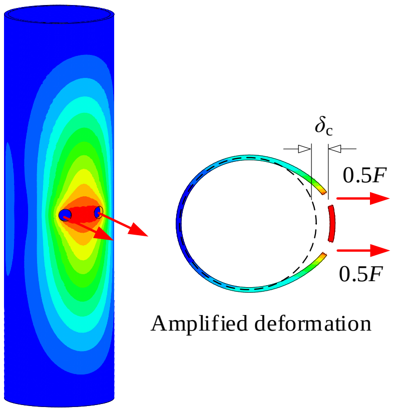

Fig. 11 Deformation of CFCT column

The load value was taken as 1 N since only elastic deformation was desired. As such, material property with only elastic behaviour was used for steel and concrete. The translations at both ends of the column were restrained as shown in Fig. 10(b). The contact interaction between concrete and steel tube was generated using the surface-to-surface technique where hard contact and penalty friction formulation were employed. Meanwhile, solid elements(C3D8I) with incompatible modes were adopted for steel tube and concrete to achieve more accurate results for flexural models and avoid shear locking effects.

Fig. 11 indicates the deflections of CFCT column subjected to tension. The deformation values at the bolt hole were captured in FEM. As can be seen, the large deformations mainly concentrated in the regions between two bolt holes as an elliptical shape which slightly differed from the CFST columns reported by Thai and Uy (2016). The stiffness coefficient of column face in bending can be thus defined as

$$k_4 = \frac{F}{E\delta_c} \tag{13}$$

where E is Young's modulus of steel tube.

4.5 Validation of modified method

To improve the accuracy of prediction, a series of stiffness coefficients in components had been modified, which include:

(1) The stiffness coefficient of endplate in bending had been revised by reducing the factor from 0.9 to 0.68;
(2) The stiffness coefficient of bolts in tension had been amplified by considering an angle between the axial direction of bolts and the direction of tensile load;
(3) Contribution of profiled sheeting in tension had

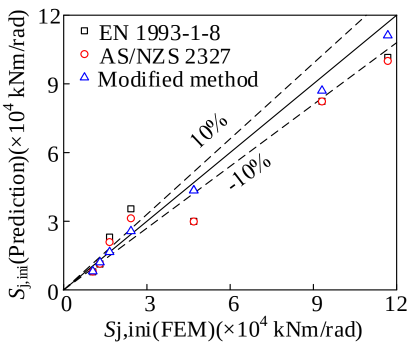

(a) Carbon steel

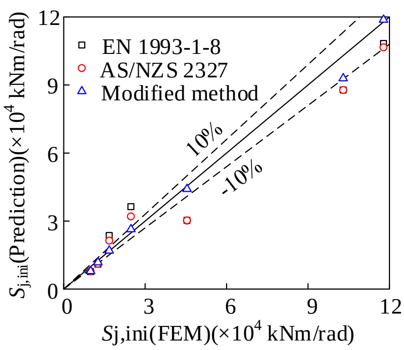

(b) Finite element model

Fig. 12 Comparison of initial stiffness between FEM and predictions been included in the reinforcement in tension if the sheeting rib is along the direction of beam flanges;

(4) The stiffness coefficient of column face in bending had been estimated based on actual numerical results.

Afterwards, the initial stiffness of composite joints with carbon steel and stainless steel was re-estimated based on the modified component method. The comparisons are outlined in Table 6 and Fig. 12. It can be found that the improvement was significant where the mean value of ratio reached 0.97 and 0.99 for carbon steel and stainless steel. Moreover, the standard deviation reduced to 0.05, which revealed a rational prediction. Overall, the modified component method is reliable to evaluate the initial stiffness of composite beam-to-CFCT column joints with not only carbon steel but also stainless steel.

5. Numerical analysis of column face in bending

To make the modified method more practical and straightforward for designers predicting the flexural performance of composite joints with circular columns, it is necessary to update the stiffness coefficient of column face in bending by AS/NZS 2327. In this case, a wide range of

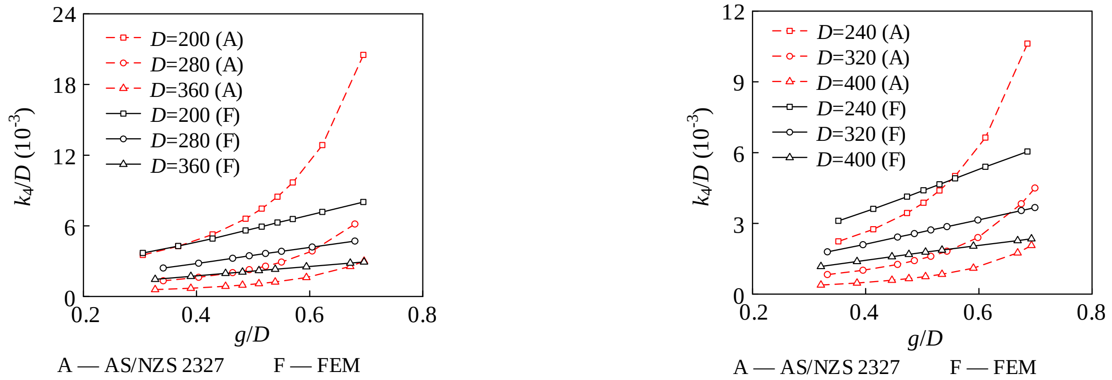

Fig. 13 Comparison of stiffness coefficient in terms of g/D

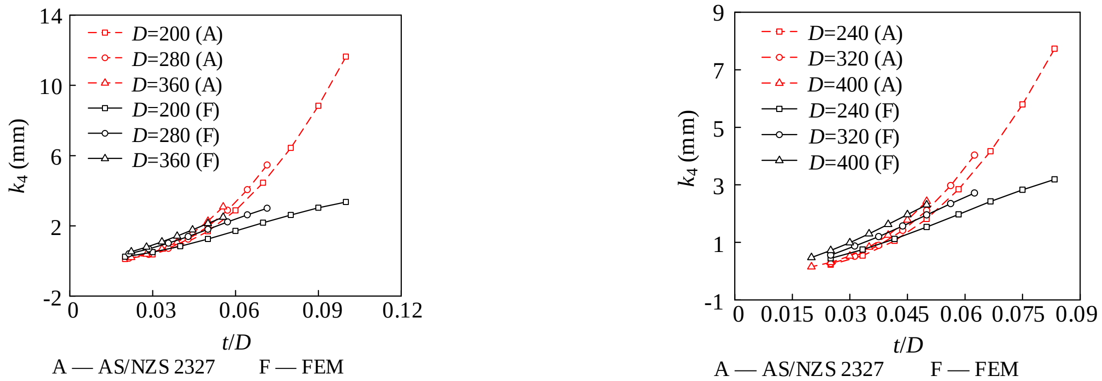

Fig. 14 Comparison of stiffness coefficient in terms of t/D

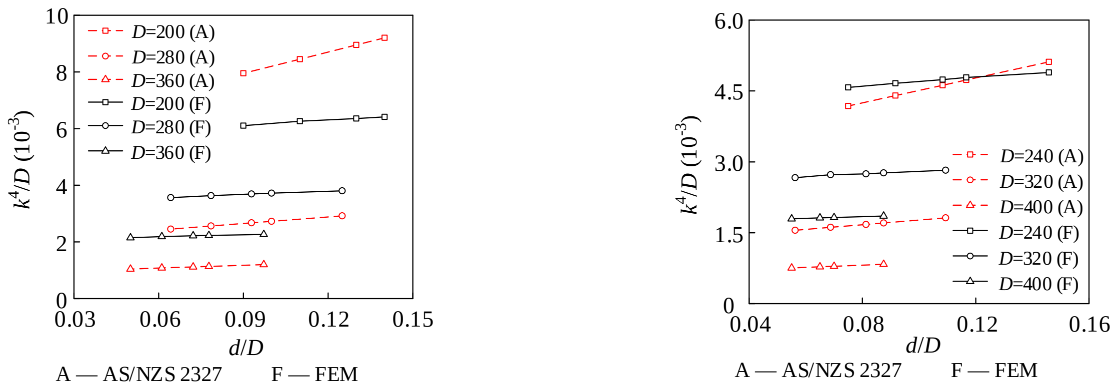

Fig. 15 Comparison of stiffness coefficient in terms of d/D

numerical models need to be created to investigate the stiffness coefficient under various parameters such as the diameter of column (D), diameter of bolt holes (d), thickness of column wall (t) and space between two bolt holes (g). The details are summarised in Table A at Appendix. The dimensions of benchmark models in each group that possess the same diameter of column were highlighted in bold. In addition, the parameters were limited within a specific range indicated in Fig. 10(a) according to Thai and Uy (2016).

Due to the fact that 126 numerical models in total were developed, it is quite labour intensive and time consuming to create geometric configurations through the ABAQUS interface operation. However, ANSYS (2019) provides a sufficient way to save time owing to its convenient and powerful script function. As such, the pre-process of modelling was conducted by ANSYS including geometry generation, material property, meshing, boundary conditions and loading conditions. The numerical models were then transformed to ABAQUS for computing and post-process.

All components were simulated with solid elements (SOLID45) in ANSYS and were converted to C3D8I automatically in ABAQUS. The numerical results were initially verified with those mentioned in Section 4.4, and it suggested the method was reasonable and reliable.

5.1 Numerical results and discussion

All the computed stiffness coefficients by FEM were compared with those predicted by AS/NZS 2327, and the comparisons are indicated in Figs. 13-15. It can be seen in Fig. 13 that the relationship between g and k_4 obtained from FEM exhibits linear level, while significant nonlinear correlations are observed in AS/NZS 2327. In addition, there exists a high discrepancy of results between FEM and the design code. The similar observation is made in the comparison regarding the parameter t/D and k_4. Although both estimations suggest a nonlinear relationship between t/D and k_4 for a small thickness of column wall. AS/NZS 2327 extensively overestimates the coefficient when it comes to a large thickness of column wall. As for the stiffness coefficient related to the diameter of bolt holes, it can be found that k_4 is correlated with d linearly. Nonetheless, the design code underestimates the value in the whole. Overall, the deformation response of CFCT column face in bending was apparently different from CFST column face in bending, and the formula in AS/NZS 2327 regarding the column face in bending should be modified.

5.2 Regression analysis

Based on the above-mentioned discussion, the 126 numerical results were used to modify the formula by means of regression analysis. As suggested, the stiffness coefficient was related to four independent variables, and it can be fitted by a nonlinear function, namely $k_4 = f(g/D, t/D, d/D, D)$. According to the formula in AS/NZS 2327, the function specified in the design provision can be derived as

$$k_4 = \beta^3 \times \frac{A \times \gamma + B \times (1-\alpha) \times \tan\alpha}{(1-\alpha)^3 + C \times (1-\alpha) \times \beta^2} \times D \qquad (14)$$

where α, β, γ equals to g/D, t/D, d/D, respectively; A, B and C are parameters.

The expression describes a nonlinear relationship between g/D and k_4. However, the numerical simulations in Section 5.1 have clarified new relationships between independent variables and dependent variable. As such, Eq. (14) is revised through regression analysis, and parameters A, B and C can be determined as

$$k_4 = \beta^3 \times \frac{A \times \gamma + B \times \alpha}{1 + C \times \beta^2} \times D \qquad (15)$$
$$A = 58.73,\ B = 347,\ C = 1073.8$$

Figs. 16-18 denote that the regression analysis has a good agreement with numerical results, and the accuracy degree reaches 99% with a satisfactory standard deviation as shown in Fig. 19. Meanwhile, it is demonstrated in

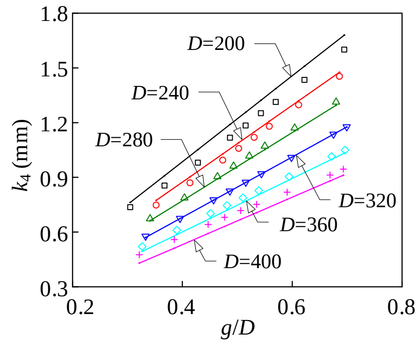

Fig. 16 Regression analysis in terms of g/D

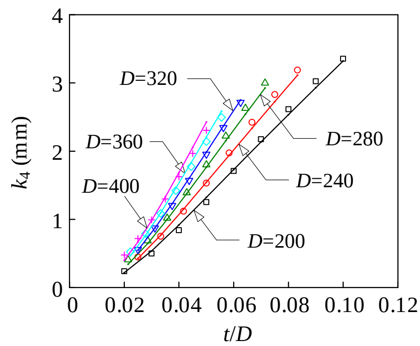

Fig. 17 Regression analysis in terms of t/D

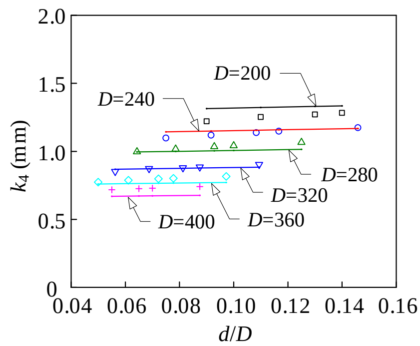

Fig. 18 Regression analysis in terms of d/D

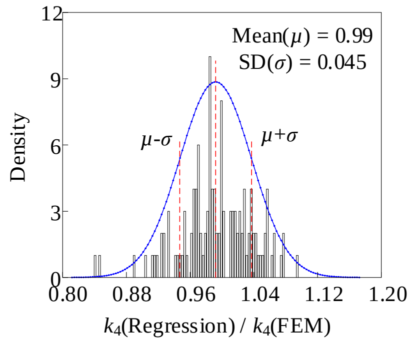

Fig. 19 Normal distribution of proposed formula

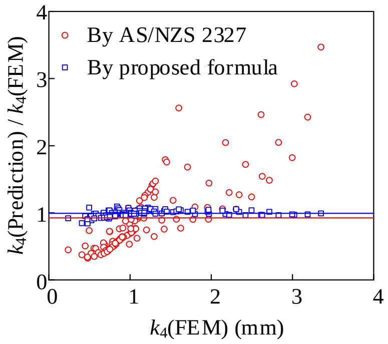

Fig. 20 Comparison of k_4 between AS/NZS 2327 and proposed formula

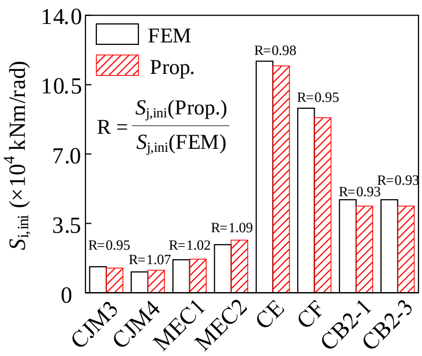

Fig. 21 Validation of proposed formula

Fig. 20 that the modified formula is able to predict the stiffness coefficient of CFCT column face in bending better than the current formula in AS/NZS 2327. The proposed formula can be applied to single-sided joints as well as double-sided joints, and the final expression can be denoted by

$$k_4 = \beta^3 \times \frac{58.73\gamma + 347\alpha}{1 + 1073.8\beta^2} \times D$$
$$0.3 \le \alpha = \frac{g}{D} \le 0.7,\ 0.02 \le \beta = \frac{t}{D} \le 0.1, \qquad (16)$$
$$0.05 \le \gamma = \frac{d}{D} \le 0.15$$

5.3 Validation of proposed formula

The initial stiffness of eight joints mentioned in Section 2 was re-evaluated based on the proposed formula to verify its rationality. Fig. 21 depicts the comparison, and it suggests that the initial stiffness remains consistent. Therefore, the proposed formula in Eq. (16) is reliable to provide design guidance.

6. Conclusions

The performance of composite beam-to-CFCT column joints made of stainless steel has been investigated by means of numerical analysis which was verified with independent experimental results. Compared with the composite joints made of carbon steel, the use of stainless steel could reduce the elastic moment range. It is found that the maximum elastic moment for stainless steel approached a half of moment capacity, while that for carbon steel could reach up to two thirds of moment capacity.

The initial stiffness and moment capacity were estimated by the existing component method from EN 1993-1-8 and AS/ZNS 2327. Various key findings are herein summarised:

- The existing design codes underestimate the moment capacity and initial stiffness of composite beam-to-CFCT column joints, although the slightly better estimations are observed in AS/NZS 2327.
- The standard T-stub model is not appropriate to predict the behaviour of curved column flange and endplate in bending.
- Several modifications regarding the initial stiffness by the component method needs to be employed including the endplate in bending, bolts in tension, profiled sheeting in tension and column face in bending. The factor related to the stiffness coefficient of endplate in bending is recommended to be 0.68 for joints with CFCT columns. The stiffness coefficient of bolts in tension could be amplified by considering an angle between the axial direction of bolts and the direction of tensile load. Contribution of profiled sheeting should be considered if the sheeting rib is placed along the direction of beam flange. The stiffness coefficient of CFCT column face in bending could be newly proposed by regression analysis.

The modified component method is able to estimate the initial stiffness of beam-to-CFCT column joints with or without concrete slabs. Moreover, the proposed formula estimating the stiffness coefficient of column face in bending can be applied to single-sided and double-sided joints.

Acknowledgments

The research described in this paper is financially supported by the Australian Research Council (ARC) under its Discovery Scheme (Project No: DP180100418). The financial support is gratefully acknowledged. The authors acknowledge the University of Sydney HPC service for providing resources that have contributed to the research results in this paper.

References

ABAQUS (2016), User Manual. Version 6.16, DS SIMULIA Corp, Providence, RI, USA.

Amadio, C., Bedon, C., Fasan, M. and Pecce, M.R. (2017), "Refined numerical modelling for the structural assessment of steel-concrete composite beam-to-column joints under seismic loads", *Eng. Struct.*, **138**, 394-409. https://doi.org/10.1016/j.engstruct.2017.02.037

ANSYS® Academic Research Mechanical, Release 2019R1

AS/NZS 2327-2017 (2017), Composite structures—Composite steel-concrete construction in buildings; Australia.

Averseng, J., Bouchair, A. and Chateauneuf, A. (2017), "Reliability analysis of the nonlinear behaviour of stainless steel cover-plate joints", *Steel Compos. Struct., Int. J.*, **25**(1), 45-55. https://doi.org/10.12989/scs.2017.25.1.045

Cai, Y. and Young, B. (2019), "Experimental investigation of carbon steel and stainless steel bolted connections at different strain rates", *Steel Compos. Struct., Int. J.*, **30**(6), 551-565. https://doi.org/10.12989/scs.2019.30.6.551

Costa, R., Valdez, J., Oliveira, S., da Silva, L.S. and Bayo, E. (2019), "Experimental behaviour of 3D end-plate beam-to-column bolted steel joints", *Eng. Struct.*, **188**, 277-289. https://doi.org/10.1016/j.engstruct.2019.03.017

Dai, X. and Lam, D. (2010), "Axial compressive behaviour of stub concrete-filled columns with elliptical stainless steel hollow sections", *Steel Compos. Struct., Int. J.*, **10**(6), 517-539. https://doi.org/10.12989/scs.2010.10.6.517

Díaz, C., Victoria, M., Querin, O.M. and Martí, P. (2018), "FE model of three-dimensional steel beam-to-column bolted extended end-plate joint", *Int. J. Steel Struct.*, **18**, 843-867. https://doi.org/10.1007/s13296-018-0033-y

Ding, F.X., Yin, Y.X., Wang, L., Yu, Y., Luo, L. and Yu, Z.W. (2019), "Confinement coefficient of concrete-filled square stainless steel tubular stub columns", *Steel Compos. Struct., Int. J.*, **30**(4), 337-350. https://doi.org/10.12989/scs.2019.30.4.337

Elflah, M., Theofanous, M., Dirar, S. and Yuan, H. (2019a), "Behaviour of stainless steel beam-to-column joints—Part 1: Experimental investigation", *J. Constr. Steel Res.*, **152**, 183-193. https://doi.org/10.1016/j.jcsr.2018.02.040

Elflah, M., Theofanous, M., Dirar, S. and Yuan, H. (2019b), "Structural behaviour of stainless steel beam-to-tubular column joints", *Eng. Struct.*, **184**, 158-175. https://doi.org/10.1016/j.engstruct.2019.01.073

EN 1993-1-8 (2005), Eurocode 4: Design of steel structures. part 1–8: design of joints; Brussels, Belgium: European Committee for Standardization.

EN 1994-1-1 (2004), Eurocode 4: Design of composite steel and concrete structures. part 1–1: general rules and rules for buildings; Brussels, Belgium: European Committee for Standardization.

Francavilla, A.B., Latour, M., Piluso, V. and Rizzano, G. (2018), "Design of full-strength full-ductility extended end-plate beam-to-column joints", *J. Constr. Steel Res.*, **148**, 77-96. https://doi.org/10.1016/j.jcsr.2018.05.013

Gardner, L., Bu, Y., Francis, P., Baddoo, N.R., Cashell, K.A. and McCann, F. (2016), "Elevated temperature material properties of stainless steel reinforcing bar", *Constr. Build. Mater.*, **114**, 977-997. https://doi.org/10.1016/j.conbuildmat.2016.04.009

Gil, B., Goñi, R. and Bayo, E. (2013), "Experimental and numerical validation of a new design for three-dimensional semi-rigid composite joints", *Eng. Struct.*, **48**, 55-69. https://doi.org/10.1016/j.engstruct.2012.08.034

Hoang, V.L., Demonceau, J.F. and Jaspart, J.P. (2014), "Resistance of through-plate component in beam-to-column joints with circular hollow columns", *J. Constr. Steel Res.*, **92**, 79-89. https://doi.org/10.1016/j.jcsr.2013.10.001

Jeyarajan, S. and Liew, J.R. (2016), "Robustness analysis of 3D Composite buildings with semi-rigid joints and floor slab", *Structures*, **6**, 20-29. https://doi.org/10.1016/j.istruc.2016.01.005

Lai, Z., Fischer, E.C. and Varma, A.H. (2019), "Database and Review of Beam-to-Column Connections for Seismic Design of Composite Special Moment Frames", *J. Struct. Eng.*, **145**(5), 04019023. https://doi.org/10.1061/(ASCE)ST.1943-541X.0002295

Lan, X., Huang, Y., Chan, T.M. and Young, B. (2018), "Static strength of stainless steel K-and N-joints at elevated temperatures", *Thin-Wall. Struct.*, **122**, 501-509. https://doi.org/10.1016/j.tws.2017.10.009

Li, D.X., Uy, B. and Wang, J. (2019), "Behaviour and design of high-strength steel beam-to-column joints", *Steel Compos. Struct., Int. J.*, **31**(3), 303-317. https://doi.org/10.12989/scs.2019.31.3.303

Liew, J.R., Teo, T.H. and Shanmugam, N.E. (2004), "Composite joints subject to reversal of loading—Part 2: analytical assessments", *J. Constr. Steel Res.*, **60**(2), 247-268. https://doi.org/10.1016/j.jcsr.2003.08.011

Mirambell, E. and Real, E. (2000), "On the calculation of deflections in structural stainless steel beams: an experimental and numerical investigation", *J. Constr. Steel Res.*, **54**(1), 109-133. https://doi.org/10.1016/S0143-974X(99)00051-6

Mursi, M. and Uy, B. (2003), "Strength of concrete filled steel box columns incorporating interaction buckling", *J. Struct. Eng.*, **129**(5), 626-639. https://doi.org/10.1061/(ASCE)0733-9445(2003)129:5(626)

Qiang, X., Bijlaard, F.S., Kolstein, H. and Jiang, X. (2014), "Behaviour of beam-to-column high strength steel endplate connections under fire conditions–Part 1: Experimental study", *Eng. Struct.*, **64**, 23-38. https://doi.org/10.1016/j.engstruct.2014.01.028

Ramberg, W. and Osgood, W.R. (1943), "Description of stress–strain curves by three parameters", Technical Note No. 902, National Advisory Committee for Aeronautics, Washington DC, USA.

Shams, M. and Saadeghvaziri, M.A. (1999), "Nonlinear response of concrete-filled steel tubular columns under axial loading", *Struct. J.*, **96**(6), 1009-1017.

Song, T.Y., Tao, Z., Razzazzadeh, A., Han, L.H. and Zhou, K. (2017), "Fire performance of blind bolted composite beam to column joints", *J. Constr. Steel Res.*, **132**, 29-42. https://doi.org/10.1016/j.jcsr.2017.01.011

Song, Y.C., Uy, B. and Wang, J. (2019), "Numerical analysis of stainless steel-composite beam-to-column joints with bolted flush endplates", *Steel Compos. Struct., Int. J.*, **33**(1), 143-162. https://doi.org/10.12989/scs.2019.33.1.143

Tao, Z., Hassan, M.K., Song, T.Y. and Han, L.H. (2017), "Experimental study on blind bolted connections to concrete-filled stainless steel columns", *J. Constr. Steel Res.*, **128**, 825-838. https://doi.org/10.1016/j.jcsr.2016.10.016

Thai, H.T. and Uy, B. (2016), "Rotational stiffness and moment resistance of bolted endplate joints with hollow or CFST columns", *J. Constr. Steel Res.*, **126**, 139-152. https://doi.org/10.1016/j.jcsr.2016.07.005

Thai, H.T., Uy, B. and Aslani, F. (2017), "Behaviour of bolted endplate composite joints to square and circular CFST columns", *J. Constr. Steel Res.*, **131**, 68-82.

https://doi.org/10.1016/j.jcsr.2016.12.022

Theofanous, M. and Gardner, L. (2012), “Effect of element interaction and material nonlinearity on the ultimate capacity of stainless steel cross-sections”, *Steel Compos. Struct., Int. J.*, **12**(1), 73-92. https://doi.org/10.12989/scs.2011.12.1.073

Tizani, W., Wang, Z.Y. and Hajirasouliha, I. (2013), “Hysteretic performance of a new blind bolted connection to concrete filled columns under cyclic loading: An experimental investigation”, *Eng. Struct.*, **46**, 535-546. https://doi.org/10.1016/j.engstruct.2012.08.020

Wang, J.F. and Chen, L. (2012), “Experimental investigation of extended end plate joints to concrete-filled steel tubular columns”, *J. Constr. Steel Res.*, **79**, 56-70. https://doi.org/10.1016/j.jcsr.2012.07.016

Wang, J.F. and Zhang, N. (2017), “Performance of circular CFST column to steel beam joints with blind bolts”, *J. Constr. Steel Res.*, **130**, 36-52. https://doi.org/10.1016/j.jcsr.2016.11.026

Wang, J.F., Han, L.H. and Uy, B. (2009), “Behaviour of flush end plate joints to concrete-filled steel tubular columns”, *J. Constr. Steel Res.*, **65**(4), 925-939. https://doi.org/10.1016/j.jcsr.2008.10.010

Wang, Z.Y., Tizani, W. and Wang, Q.Y. (2010), “Strength and initial stiffness of a blind-bolt connection based on the T-stub model”, *Eng. Struct.*, **32**(9), 2505-2517. https://doi.org/10.1016/j.engstruct.2010.04.005

Wang, J., Uy, B. and Li, D. (2018a), “Analysis of demountable steel and composite frames with semi-rigid bolted joints”, *Steel Compos. Struct., Int. J.*, **28**(3), 363-380. https://doi.org/10.12989/scs.2018.28.3.363

Wang, J., Zhu, H., Uy, B., Patel, V., Aslani, F. and Li, D. (2018b), “Moment-rotation relationship of hollow-section beam-to-column steel joints with extended end-plates”, *Steel Compos. Struct., Int. J.*, **29**(6), 717-734. https://doi.org/10.12989/scs.2018.29.6.717

Wang, J., Uy, B. and Li, D.X. (2019), “Behaviour of large fabricated stainless steel beam-to-tubular column joints with extended endplates”, *Steel Compos. Struct., Int. J.*, **32**(1), 141-156. https://doi.org/10.12989/scs.2019.32.1.141

Weynand, K., Jaspart, J.P. and Steenhuis, M. (1996), “The stiffness model of revised Annex J of Eurocode 3”, *Proceedings of the Third International Workshop on Connections in Steel Structures*, pp. 441-452, Pergamon, Turkey.

Yang, B. and Tan, K.H. (2013), “Behaviour of composite beam-column joints in a middle-column-removal scenario: experimental tests”, *J. Struct. Eng.*, **140**(2), 04013045. https://doi.org/10.1061/(ASCE)ST.1943-541X.0000805

Yang, J., Sheehan, T., Dai, X.H. and Lam, D. (2015), “Experimental study of beam to concrete-filled elliptical steel tubular column connections”, *Thin-Wall. Struct.*, **95**, 16-23. https://doi.org/10.1016/j.tws.2015.06.009

Yee, Y.L. and Melchers, R.E. (1986), “Moment-rotation curves for bolted connections”, *J. Struct. Eng.*, **112**(3), 615-635. https://doi.org/10.1061/(ASCE)0733-9445(1986)112:3(615)

Zeng, J., Lu, W. and Paavola, J. (2018), “Ultimate strength of a beam-to-column joint in a composite slim floor frame”, *J. Constr. Steel Res.*, **140**, 82-91. https://doi.org/10.1016/j.jcsr.2017.10.009

DL

Appendix

Table A Details of parameters (Unit: mm)

D	*d*	*t*	*g*	*d*/*D*	k_4	*t*/*D*	k_4	*g*/*D*	k_4
200	18	4	61.0	0.09	1.2210	0.02	0.2379	0.3051	0.7361
	22	6	73.5	0.11	1.2519	0.03	0.4975	0.3676	0.8547
	26	8	85.7	0.13	1.2706	0.04	0.8402	0.4283	0.9805
	28	**10**	97.4	0.14	1.2828	0.05	1.2519	0.4869	1.1170
		12	103.1			0.06	1.7086	0.5153	1.1835
		14	**108.6**			0.07	2.1754	0.5431	1.2519
		16	114.1			0.08	2.6149	0.5703	1.3126
		18	124.5			0.09	3.0236	0.6224	1.4337
		20	139.0			0.10	3.3532	0.6949	1.6001
240	18	6	84.5	0.075	1.0977	0.025	0.4473	0.3523	0.7476
	22	8	99.3	0.092	1.1187	0.033	0.7512	0.4139	0.8693
	26	**10**	113.6	0.108	1.1372	0.042	1.1187	0.4735	0.9939
	28	12	120.6	0.117	1.1481	0.05	1.5310	0.5025	1.0583
	35	14	**127.4**	0.146	1.1734	0.058	1.9731	0.5308	1.1187
		16	134.1			0.067	2.4235	0.5586	1.1793
		18	146.9			0.075	2.8297	0.6119	1.2971
		20	164.7			0.083	3.1884	0.6862	1.4529
280	18	6	95.6	0.064	0.9975	0.021	0.4062	0.3413	0.6729
	22	8	113.0	0.079	1.0171	0.029	0.6847	0.4036	0.7874
	26	**10**	129.9	0.093	1.0340	0.036	1.0171	0.4640	0.9036
	28	12	138.1	0.1	1.0412	0.043	1.3909	0.4933	0.9622
	35	14	**146.2**	0.125	1.0656	0.05	1.7997	0.5221	1.0171
		16	154.1			0.057	2.2207	0.5502	1.0713
		18	169.2			0.064	2.6277	0.6044	1.1709
		20	190.4			0.071	2.9975	0.6800	1.3133
320	18	8	106.6	0.056	0.8524	0.025	0.5566	0.3331	0.5769
	22	**10**	126.7	0.069	0.8734	0.031	0.8734	0.3959	0.6750
	26	12	146.2	0.081	0.8790	0.038	1.2030	0.4568	0.7764
	28	14	155.7	0.088	0.8850	0.044	1.5706	0.4865	0.8245
	35	16	**165.0**	0.109	0.9033	0.05	1.9550	0.5155	0.8734
		18	174.1			0.056	2.3441	0.5439	0.9198
		20	191.6			0.063	2.7156	0.5987	1.0093
			216.1					0.6754	1.1367
			223.8					0.6993	1.1766
360	18	8	117.6	0.05	0.7731	0.022	0.5254	0.3267	0.5203
	22	**10**	140.4	0.061	0.7876	0.028	0.7876	0.3899	0.6109
	26	12	162.5	0.072	0.7976	0.033	1.0860	0.4513	0.7019
	28	14	173.2	0.078	0.8019	0.039	1.4202	0.4811	0.7455
	35	16	**183.7**	0.097	0.8161	0.044	1.7740	0.5104	0.7876
		18	194.1			0.05	2.1394	0.5390	0.8279
		20	214.0			0.056	2.4961	0.5943	0.9040
			241.8					0.6717	1.0142
			250.5					0.6960	1.0499

Table A Continued

D	d	t	g	d/D	k_4	t/D	k_4	g/D	k_4
	22	8	128.6	0.055	0.7179	0.02	0.4769	0.3216	0.4751
	26	**10**	154.1	0.065	0.7255	0.025	0.7179	0.3852	0.5591
	28	12	178.7	0.07	0.7291	0.03	0.9914	0.4468	0.6417
	35	14	190.7	0.088	0.7413	0.035	1.2981	0.4768	0.6807
400		16	**202.5**			0.04	1.6250	0.5063	0.7179
		18	214.1			0.045	1.9667	0.5351	0.7523
		20	236.3			0.05	2.3063	0.5908	0.8189
			267.5					0.6689	0.9124
			277.3					0.6933	0.9451